chemistry proceedings

MDPI

Proceeding Paper

"TYC" Reaction between Alkynes and Catechol-Thiol Derivatives Prompted by Metal Nanocatalysis: Mechanism Study by DFT Calculation †

Matías Capurso, Gabriel Radivoy, Fabiana Nador and Viviana Dorn *

Instituto de Química del Sur (INQUISUR-CONICET), Depto. de Química, Universidad Nacional del Sur, Av. Alem 1253, Bahía Blanca B8000CPB, Argentina; matias.capurso@uns.edu.ar (M.C.); email1@gmail.com (G.R.); email2@gmail.com (F.N.)

* Correspondence: vdorn@uns.edu.ar

† Presented at the 26th International Electronic Conference on Synthetic Organic Chemistry; Available online: https://ecsoc-26.sciforum.net.

Abstract: A recently published article by our research group demonstrated that the hydrothiolation of activated alkynes is a successful way to functionalize thiols bearing catechols. The reaction was promoted by the CuNPs/TiO_2 nanocatalyst and resulted regio- and stereoselective towards the *anti*-Markovnikov *Z*-vinyl sulfide with good to excellent yields (47–97%). The scope of the reaction was evaluated, and based on experimental observations, the reaction mechanism was investigated through DFT studies. Theoretical results and experimental data were consistent with a reaction mechanism based on a copper-catalyzed *anti*-Markovnikov hydrothiolation process that favors the formation of the *Z*-vinyl sulfide.

Keywords: hydrothiolation; DFT; computational chemistry

Citation: Capurso, M.; Radivoy, G.; Nador, F.; Dorn, V. "TYC" Reaction between Alkynes and Catechol-Thiol Derivatives Prompted by Metal Nanocatalysis: Mechanism Study by DFT Calculation. *Chem. Proc.* **2022**, *4*, x. https://doi.org/10.3390/xxxxx

Academic Editor(s): Julio A. Seijas

Published: 15 November 2022

Publisher's Note: MDPI stays neutral with regard to jurisdictional claims in published maps and institutional affiliations.

1. Introduction

Alkenyl sulfides are recognized constituents of the sulfur containing organic compounds and they are of great interest because they can be used as versatile building blocks in organic synthesis [1]. The alkyne hydrothiolation is a simple approach to produce alkenyl sulfides from thiols and alkynes. This reaction can be promoted by free radicals [2], strong acids [3] or bases [4] and can lead to one of the regio- and stereoisomeric alkenyl sulfides through a Markovnikov orientation (product A, Scheme 1), or give mixtures of *E*- and *Z*-isomers through an *anti*-Markovnikov orientation (products B and C, Scheme 1).

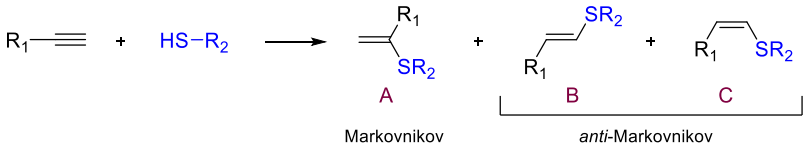

Scheme 1. Schematic representation of alkyne hydrothiolation.

Alternatively, metal catalysts have the potential to offer a high degree of regio and stereoselectivity in alkyne hydrothiolation reaction. In a recent publication [5], we informed the direct synthesis of vinyl sulfides via the Thiol-yne click reaction with activated alkynes (alkynes with electron withdrawing groups) to functionalize thiols bearing catechols. The reaction was promoted by a heterogeneous catalyst composed of copper nanoparticles supported on TiO_2 (CuNPs/TiO_2) in 1,2-dichloroethane (1,2-DCE) under heating at 80 °C. This reaction was regio- and stereoselective towards *anti*-Markovnikov *Z*-vinyl sulfide in most cases studied. However, when the reaction was carried out with alkynes

with an electron donating group, it was not occurred. Likewise, when the catalyst based on CuNPs was replaced by FeNPs, no vinyl sulfide or low conversions to the product were observed. With the aim to explain these experimental results and find a close understanding of the system, density functional theory (DFT) calculations were performed.

2. Methods

2.1. Computational Methods

Calculations were performed in ORCA version 4.2.1 [6]. All geometries were optimized in the gas phase using the PBE density functional theory method [7] with D3BJ dispersion correction [8] and the double-ζ def2-SVP basis set for all atoms [9]. For open-shell systems, the unconstrained formalism was adopted. Harmonic frequency calculations were carried out at the same level of theory in order to identify each stationary point. All charges shown are from CHELPG calculations [10].

The electronic energies were then improved through single point calculations with triple-ζ def2-TZVP basis set [9] and solvent effects introduced through the implicit solvation model CPCM [11] for the experimental solvent dichloromethane (DCM) with a dielectric constant of 9.08 as provided in the library of solvents of ORCA 4.2.1.

2.2. Experimental Methods

All moisture sensitive reactions were carried out under a nitrogen atmosphere. Anhydrous tetrahydrofuran was freshly distilled from sodium/benzophenone ketyl. All starting materials were of the best available grade (Aldrich (St. Louis, MI, USA), Merck (Darmstadt, Germany), Alfa Aesar (Haverhill, MA, USA)) and were used without further purification. Commercially available copper(II) chloride dihydrate and iron(III) chloride hexahydrate were dehydrated upon heating in oven (150 °C, 45 min) prior to use. Column chromatography was performed with Merck silica gel 60 (0.040–0.063 μm, 240–400 mesh) and hexane/EtOAc as eluent. Reactions were monitored by thin-layer chromatography on silica gel plates (60F-254) visualized under UV light and/or using $FeCl_3$ in water as stain. NMR spectra were recorded on a Bruker ARX-300 spectrometer using $CDCl_3$ or CD_3OD as solvents.

Experimental details for the reactions and preparation of the copper-nanocatalysts and reagents are reported in our previous work [5]. Except for the preparation of $FeNPs/TiO_2$ catalyst detailed below.

Preparation of $FeNPs/TiO_2$ catalyst

Anhydrous iron(III) chloride (127 mg, 1 mmol) was added to a suspension of lithium (21 mg, 3 mmol) and 4,4′-di-tert-butylbiphenyl (DTBB, 27 mg, 1 mmol) in THF (2 mL) at room temperature under a nitrogen atmosphere. This suspension was diluted with THF (3 mL) followed by the addition of the TiO_2 (800 mg). The resulting mixture was stirred for 1 h at room temperature. The solid was successively washed with EtOH and diethyl ether and dried under vacuum.

3. Results and Discussion

The alkyne hydrothiolation reaction was tested using propiolamide and 3-((4-mercaptobutyl)thio)benzene-1,2-diol, as model substrates, in the presence of $CuNPs/TiO_2$ catalyst, giving a conversion to the vinyl sulfide of 87 % and a stereo-selectivity to *Z*-vinylsulfide (*Z*/*E* ratio = 86/14) (Scheme 2).

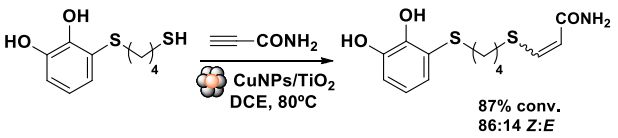

Scheme 2. Hydrothiolation reaction with the model substrates.

When the nanocatalyst was changed to FeNPs/TiO_2, no product was obtained, recovering the starting substrates. In line with our previous studies [12], we modeled three different structures for the iron nanocatalyst, considering in this case, the three possible spin states of the zero-valent iron (Figure 1).

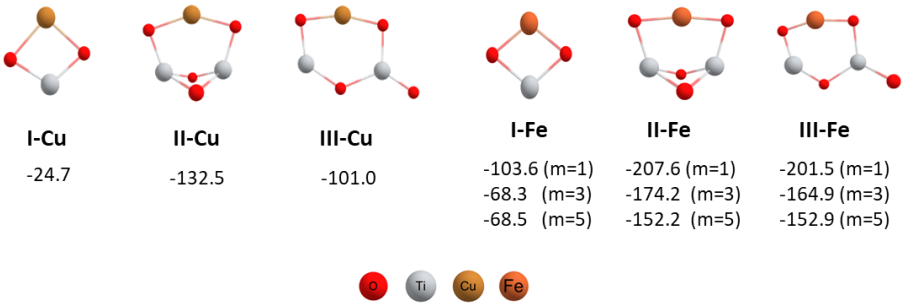

Figure 1. Geometries and formation energies in kcal/mol for the different catalysts modeled, multiplicities for iron catalysts are indicated in parentheses (PBE-D3BJ/Def2-TZVP/CPCM = DCM).

All calculated structures were stable and the formation of all of them occurred exothermically. As can be seen in Figure 1, no significant changes were observed in the optimized geometries of the iron whit regard to the copper nanocatalysts. The formation of the copper nanocatalysts were less exothermic than the iron ones. Between the simulated geometries for iron nanocatalyst, the low spin S = 0 (m = 1) state was approximately 35–40 kcal/mol more stable than the high-spin ones (m = 3 and m = 5). Besides, II-Fe and III-Fe geometries, which contained two TiO_2 units, were almost 100 kcal/mol more stable than I-Fe structure. As the same with copper nanocatalysts, structure II was also the most stable in the case of the iron nanocatalyst.

In the hydrothiolation of propiolamide with the copper nanocatalyst, we assumed that the reaction could start when the propiolamide was activated by the catalyst, so it was necessary to establish how this ligand attached to the metal. As can be seen from Figure 2, the plane monomer (I-Cu) and the most stable dimer structure (II-Cu) were considered in the formation of the π-complex with propiolamide. The formation of both complexes was thermodynamically favorable, being I-Cu-Amide the most exothermic. In both cases a H-bond interaction was observed between the *H*N- and one of the oxygen atoms of the TiO_2, with the interaction being stronger in complex II-Cu-Amide.

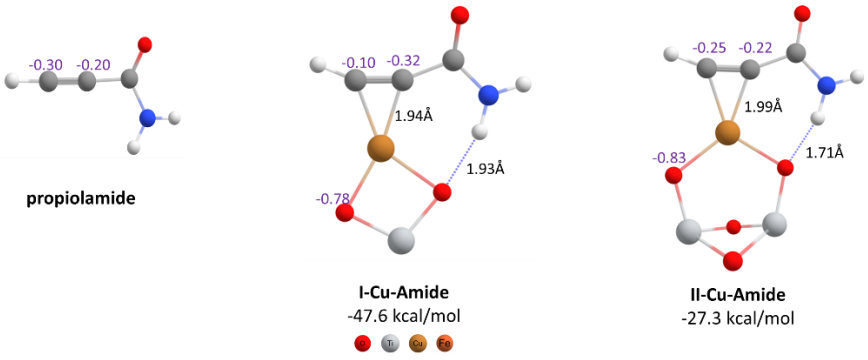

Figure 2. Geometries of propiolamide and its π-complexes with copper nanocatalysts. The formation energies, the CHELPG atomic charges and some important interatomic distances are indicated (PBE-D3BJ/Def2-TZVP/CPCM = DCM).

Regarding the charge distribution on the π-complex, the charge in the carbons of the triple bond were different. The carbon attached to the C=O became more negative, going from −0.20 in the free amide to −0.32 in I-Cu-Amide and −0.22 in II-Cu-Amide (Figure 2). On the other hand, the terminal carbon became more positive, going from −0.30 in the free

amide to −0.10 and −0.25 in the complexes respectively. This charge distribution would favor the nucleophilic attack of the thiol.

Besides the metal, the catalyst support has a non-innocent participation in the mechanism since no vinyl sulfide was obtained when the reaction was done only with $CuCl_2$ [5]. Catechol fragments can coordinate with the surface titanium atoms of support facilitating its encounter with the alkyne [13]. Due to the oxygen atoms of TiO2 support, develop a significant negative charge in both complexes (−0.78 and −0.83, Figure 2), they could act as a base to deprotonate the thiol to thiolate, that would act as a strong nucleophile on the C-sp atom.

When the same reaction was tested with propargylamine (a deactivated alkyne) in the same conditions, no product was obtained. To explain this result, as can be seen from Figure 3, we modeled in a first instance, the π-complexes between the amine and the copper nanocatalysts. As above, the formation of both complexes was thermodynamically favorable, being the complex I-Cu-Amine more exothermic than II-Cu-Amine. The H-bond interactions were also observed between the *H*N- and one of the oxygen atoms of the TiO_2 for both complexes, although these interactions were weaker than the same interactions for the amide-complexes (Figure 2). Regarding the charge distribution, it was observed that beyond the terminal Csp of propargylamine became less negative after formation of complexes I-Cu-Amine and II-Cu-Amine (−0.31 and −0.40, Figure 3), this value was still very negative compared to the amide complexes (Cu-I-Amide and Cu-II-Amide). This fact would hinder the subsequent nucleophilic attack by the activated thiol on these C-sp atom, and could possibly explain why this reaction did not experimentally take place.

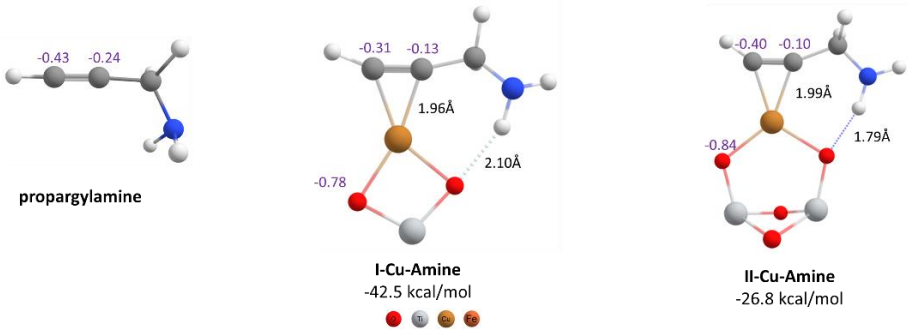

Figure 3. Geometries of propargylamine and its π-complexes with copper catalysts. Formation energies, CHELPG atomic charges and some important interatomic distances are indicated. (PBE-D3BJ/Def2-TZVP/CPCM = DCM).

As mentioned above, when the alkyne hydrothiolation was carried out with $FeNPs/TiO_2$ instead of $CuNPs/TiO_2$ nanocatalyst, no vinyl sulfide was obtained. To explain this result, we modeled the complexes between the propiolamide and the iron nanocatalysts, taking as reference the most stable structures that we had already found. As can be seen from Figure 4, formation of both complexes was thermodynamically favorable, I-Fe-Amide being approximately 15 kcal/mol more favorable than the formation of the same complex with the copper catalyst (I-Cu-Amide). In the case of the II-Fe-Amide complex, it was only 1 kcal/mol more stable than its pair with copper (II-Cu-Amide). With the aim to find an explanation in the reactivity differences between copper and iron nanocatalysts, we proceeded to explore the Fe-Amide complexes in more detail. The structure I-Fe-Amide showed a 90° rotation of the nanocatalyst compared to I-Cu-Amide complex. Moreover, the charge distribution on C-sp atoms was distinctively different from Cu-Amide complexes, because of the less negative C-sp atom was the internal one, for both I-Fe-Amide and II-Fe-Amide (−0.05 and −0.01 respectively). From this charge distribution, considering a nucleophilic attack as the next step in the mechanism, it would not be possible to obtain an anti-Markovnikov product from Fe/TiO_2 nanocatalyst.

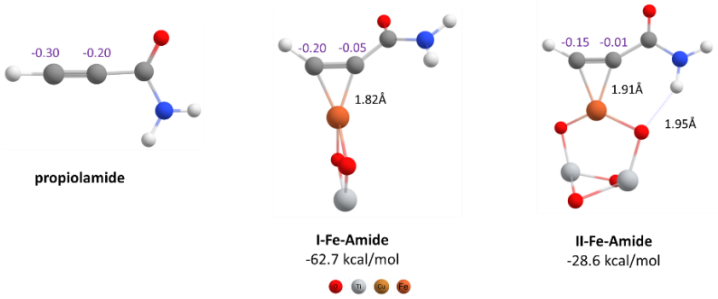

Figure 4. Geometries of propiolamide and its π-complexes with iron nanocatalysts. Formation energies, CHELPG atomic charges and some important interatomic distances are indicated (PBE-D3BJ/Def2-TZVP/CPCM = DCM).

Then, we considered that, the next step could be the nucleophilic attack of the thiol on the terminal C-sp atom (π-complex), became at the rate-determining step. As can be seen from Figure 5, this attack would take place from outside or from inside to the π-complex, giving rise to two different reaction mechanisms, which would lead to the formation of the *Z*- and/or the *E*-vinyl sulfide, respectively. In an external nucleophilic attack, the triple bond of the alkyne would be coordinated with the copper atom, while the basic centers of the support (oxygen atoms), would activate the thiol, giving a more nucleophilic thiolate.

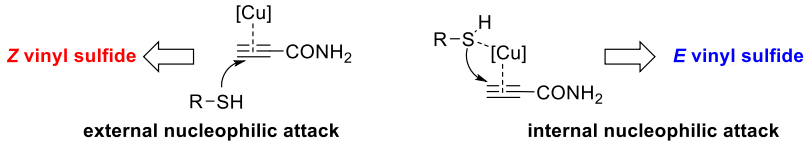

Figure 5. Possible side for the nucleophilic attack.

Taking into account these considerations, two minimal structures were modeled, a meeting complex (RC-Ext) and the subsequent intermediate (IN-Z). These two structures would occur once the external nucleophilic attack took place and would be the one that finally gives rise to the *Z*-isomer of the vinyl sulfide (Figure 6). In an internal nucleophilic attack (Figure 6), both the alkyne and the thiol would be activated again by the copper (RC-Int), the basic centers of the support (oxygen atoms) would activate the thiol, and then the nucleophilic attack, the intermediate (IN-E) would occur to finally gives rise to the *E*-isomer of the vinyl sulfide. The difference between these two mechanisms is that in the external attack, unlike the internal one, the thiol would be deprotonated by a TiO_2 of the support that would not link to the copper atom.

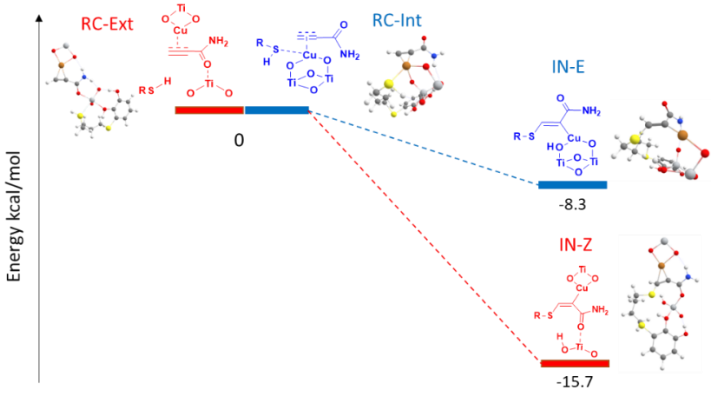

Figure 6. Potential energy profile for the external nucleophilic attack for the I-Cu-Amide complex (red) and the internal nucleophilic attack for the II-Cu-Amide complex (blue) (PBE-D3BJ/Def2-TZVP/CPCM = DCM).

As can be seen in Figure 6, when we modeled both processes, for the external and internal nucleophilic attack on the amide π-complex, we found that both routes were exothermic, favoring the formation of the expected product in *Z* and *E* configuration. However, the process that would give rise to the *Z*-vinyl sulfide took place with an exothermicity of 15.7 kcal/mol, twice the energy that was releasing for the formation of the intermediate that would give rise to the formation of the *E*-vinyl sulfide (−8.3 kcal/mol, Figure 6). These results agreed with the experimentally observed stereoselectivity.

When the same analysis was carried out for the nucleophilic attack of the amine π-complex, we found that both processes, internal and external attack, were energetically unfavorable (Figure 7). The step that would lead to the formation of the *E*-vinyl sulfide, resulted markedly endothermic, requiring process more than 20 kcal/mol. We believe that these computationally found results would explain why this reaction did not take place.

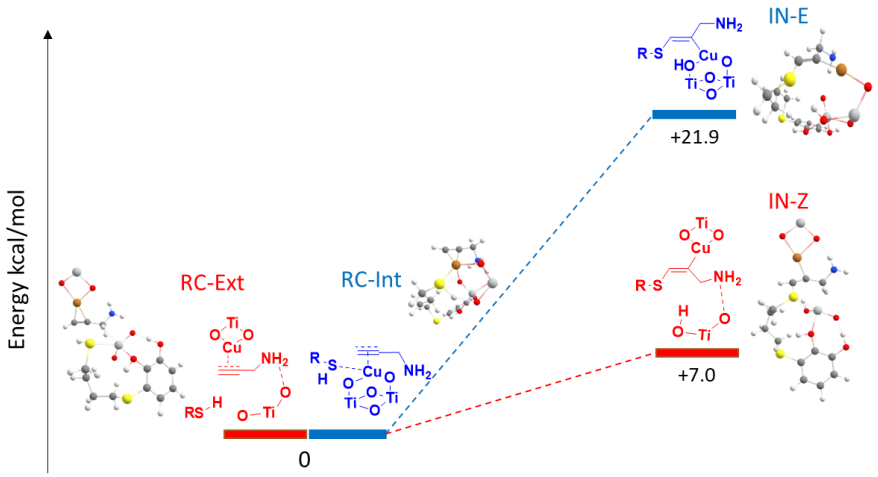

Figure 7. Potential energy profile for the external nucleophilic attack for the I-Cu-Amine complex (red) and the internal nucleophilic attack for the II-Cu-Amine complex (blue) (PBE-D3BJ/Def2-TZVP/CPCM = DCM).

4. Conclusions

We performed a computational modeling of copper and iron nanocatalyst supported on TiO_2, being II-Cu and II-Fe dimer structures the most energetically favored. Furthermore, we studied the activation of both alkynes: propiolamide and propargylamine with the copper and iron nanocatalysts. In propiolamide-copper complex a decrease of the negative charge on the terminal Csp atom would favor the subsequent nucleophilic attack of the thiol, the more negative charge on the propargylamine-copper complex on this atom would hinder the nucleophilic attack. For the propiolamide-iron complex a more positive charge at the internal carbon of the triple bond could indicate a preferring towards the Markovnikov attack, but this product was not observed experimentally. In all cases the oxygen atoms of TiO_2 support develop a significant negative charge and could act as a base to deprotonate the thiol to thiolate, that would act as a strong nucleophile.

The DFT thermochemistry modeling of the rate-determining step of the reaction, it means the nucleophilic attack, showed that the calculation methodology was robust and efficient since the results achieved were in agreement with the experimental evidence.

Further mechanistic details are now under study.

Funding: This work was generously supported by the Consejo Nacional de Investigaciones Científicas y Técnicas (CONICET, PIP N° 11220200101665CO), Agencia Nacional de Promoción Científica y Tecnológica (ANPCyT, PICT-2018-2471) and Universidad Nacional del Sur (UNS, PGI 24/Q106) from Argentina.

Data Availability Statement: Data available upon request.

Conflicts of Interest: The authors declare no conflict of interest.

References

1. (a) Doroszuk, J.; Musiejuk, M.; Ponikiewski, Ł.; Witt, D. *Eur. J. Org. Chem*. **2018**, 6333. (b) Riesco-Domínguez, A.; van de Wiel, J.; Hamlin, T.A.; van Beek, B.; Lindell, S.D.; Blanco-Ania, D.; Bickelhaupt, F.M.; Rutjes, F.P.J.T. *J. Org. Chem.* **2018**, *83*, 1779.
2. Lo Conte, M.; Pacifico, S.; Chambery, A.; Marra, A.; Dondoni, A. Synthesis of S-glycosyl amino acids and S-glycopeptides via photoinduced click thiol–ene coupling. *J. Org. Chem.* **2010**, *75*, 4644.
3. Kanagasabapathy, S.; Sudalai, A.; Benicewicz, B.C. Montmorillonite K 10-catalyzed regioselective addition of thiols and thiobenzoic acids onto olefins: An efficient synthesis of dithiocarboxylic esters. *Tetrahedron Lett.* **2001**, *42*, 3791.
4. Kondoh, K.A.; Takami, H.; Yorimitsu, K.; Oshima, J. Stereoselective Hydrothiolation of Alkynes Catalyzed by Cesium Base: Facile Access to (Z)-1-Alkenyl Sulfides. *Org. Chem.* **2005**, *70*, 6468.
5. Nador, F.; Mancebo-Aracil, J.; Thiol-yne click reaction: An interesting way to derive thiol-provided catechols. *RSC Adv.* **2021**, *11*, 2074–2082.
6. (a) Neese, F. The ORCA program system, Wiley Interdiscip. *Rev. Comput. Mol. Sci.* **2021**, *2*, 73–78. (b) Neese, F. Software update: The ORCA program system, version 4.0, Wiley Interdiscip. *Rev. Comput. Mol. Sci.* **2017**, *8*, e132.
7. Perdew, J.P.; Burke, K.; Ernzerhof, M. Generalized Gradient Approximation Made Simple. *Phys. Rev. Lett.* **1996**, *77*, 3865.
8. (a) Grimme, S.; Antony, J.; Ehrlich, S.; Krieg, H. A consistent and accurate ab initio parametrization of density functional dispersion correction (DFT-D) for the 94 elements H-Pu. *Chem. Phys.* **2010**, *132*, 154104. (b) Grimme, S.; Ehrlich, S.; Goerigk, L.J. Effect of the damping function in dispersion corrected density functional theory. *Comput. Chem.* **2011**, *32*, 1456.
9. Weigend, F.; Ahlrichs, R. Balanced basis sets of split valence, triple zeta valence and quadruple zeta valence quality for H to Rn: Design and assessment of accuracy. *Phys. Chem. Chem. Phys.* **2005**, *7*, 3297–3305.
10. Breneman, C.M.; Wiberg, K.B. Determining atom-centered monopoles from molecular electrostatic potentials. The need for high sampling density in formamide conformational analysis. *J. Comput. Chem.* **1990**, *11*, 361–373.
11. Barone, V.; Cossi, M.J. Quantum Calculation of Molecular Energies and Energy Gradients in Solution by a Conductor Solvent Model. *Phys. Chem. A* **1998**, *102*, 1995.
12. Capurso, M.; Radivoy, G.; Nador, F.; Dorn, V. Synthesis of Alkenyl Sulfides Catalyzed by CuNPs/TiO2. A Theoretical-Computational Analysis. *Chem. Proc.* **2021**, *3*, 120.
13. Li, S.; Wang, J.; Jacobson, P.; Gong, X.; Selloni, A.; Diebold, U. Correlation between Bonding Geometry and Band Gap States at Organic−Inorganic Interfaces: Catechol on Rutile TiO2(110). *J. Am. Chem. Soc.* **2009**, *131*, 980–984.